



# Unified cochlear model for low- and high-frequency mammalian hearing

Aritra Sasmal<sup>a</sup> and Karl Grosh<sup>a,b,1</sup>

<sup>a</sup>Department of Mechanical Engineering, University of Michigan, Ann Arbor, MI 48109; and <sup>b</sup>Department of Biomedical Engineering, University of Michigan, Ann Arbor, MI 48109

Edited by David P. Corey, Harvard Medical School, Boston, MA, and accepted by Editorial Board Member Charles F. Stevens May 28, 2019 (received for review January 14, 2019)

The spatial variations of the intricate cytoarchitecture, fluid scalae, and mechano-electric transduction in the mammalian cochlea have long been postulated to provide the organ with the ability to perform a real-time, time-frequency processing of sound. However, the precise manner by which this tripartite coupling enables the exquisite cochlear filtering has yet to be articulated in a base-to-apex mathematical model. Moreover, while sound-evoked tuning curves derived from mechanical gains are excellent surrogates for auditory nerve fiber thresholds at the base of the cochlea, this correlation fails at the apex. The key factors influencing the divergence of both mechanical and neural tuning at the apex, as well as the spatial variation of mechanical tuning, are incompletely understood. We develop a model that shows that the mechanical effects arising from the combination of the taper of the cochlear scalae and the spatial variation of the cytoarchitecture of the cochlea provide robust mechanisms that modulate the outer hair cell-mediated active response and provide the basis for the transition of the mechanical gain spectra along the cochlear spiral. Further, the model predicts that the neural tuning at the base is primarily governed by the mechanical filtering of the cochlear partition. At the apex, microscale fluid dynamics and nanoscale channel dynamics must also be invoked to describe the threshold neural tuning for low frequencies. Overall, the model delineates a physiological basis for the difference between basal and apical gain seen in experiments and provides a coherent description of high- and low-frequency cochlear tuning.

cochlear mechanics | low-frequency hearing | finite-element method | emergent system response | biophysics

The mammalian cochlea acts as an acoustic spectral analyzer because the emergent organ-level dynamics arising from the spatial organization of its morphological, mechanical, electrochemical, and neural characteristics impart a base-to-apex gradient of frequency selectivity known as the tonotopic map. The tuning of the sound-induced mechanical response of a key structural element of the cochlea, the basilar membrane (BM), has traditionally been used as a proxy for the auditory nerve fiber (ANF) response because of measured similarities between the 2 quantities (1). However, the canonical theory is based on experiments confined to the basal end of the cochlea, and more recent apical measurements have challenged this tenet (2, 3). For instance, experiments in the apical turn of the guinea pig cochlea using optical coherence tomography (OCT) (2) have shown that the BM response is poorly tuned and does not exhibit the high and nonlinear gain seen in the basal turn. Vibrations at a point near the reticular lamina (RL) at the apex do exhibit a 20- to 30-dB nonlinear gain shift from low to high sound pressure level (SPL) (3) but fail to recreate the “V”-shaped tuning associated with the ANF threshold (3–6). The differences between the mechanical tuning at the base and that at the apex, as well as the divergence of the mechanical and neural tuning at the apex, have given rise to the notion that the underlying micromechanics in the basal part of the mammalian cochlea are different from those of the apex, and there exists a transition from the basal to the apical mechanics along the cochlear spiral (7).

Although theoretical and numerical studies have been successful in modeling the basal, high-frequency response of the

cochlea (14–16), few studies have concentrated on modeling the cochlear response at the apex. Recently, a model that includes the feed-forward effect from the phalangeal processes was shown to provide a good fit of the vibration amplitude at the base as well as at the apex in the high-frequency hearing mouse cochlea (17). However, the model overestimates the phase accumulation observed in vivo and lacks the mechanics of the tectorial membrane (TM) which have been shown to be an important factor governing the amplification in the cochlea, both theoretically (13) and experimentally (18, 19). Other models have shown that the mechanical properties of the BM (20), impedance of the helicotrema (21–23), and curvature of the cochlea (24) could play a role in low-frequency hearing. Reichenbach and Hudspeth (25) proposed a model to account for the loss of BM amplification at the apex by critically tuning the hair bundle (HB) and the outer hair cell (OHC) electromotile feedback parameters. However, this model assumes equality of the hair bundle and transverse RL motions, which is inconsistent with experimental data (26) and higher-fidelity physiological models (12). Further, this model assumes that the positive HB deflection leads to the hyperpolarization of the hair cell which is unlikely to be true in vivo in the mammalian cochlea. Nevertheless, the model shows a possible mechanism that could decouple the BM from the HB to explain the lack of BM amplification at the apex. Although these previous studies have indicated mechanisms that could be pertinent to low-frequency hearing, none has led to the development of a global model of the cochlea that accurately predicts the diversity of gains seen across the entire range of frequencies. In this paper, we develop a physiologically based model that explains the mechanical tuning of the cochlea from base to apex.

## Significance

Developing a mathematical model that predicts the response of the cochlea over the entirety of the cochlear spiral has been an outstanding challenge in the field. Without such a model, an accurate representation of interactions occurring inside the cochlea in response to complex signals like speech sounds or tone combinations that evoke clinically relevant otoacoustic emissions is impossible. We show that incorporation of the taper of the cochlear ducts and macro- and microscale fluid viscosity along with the subtle change of the intricate cochlear cytoarchitecture into a mechano-electric-acoustic model provide the key ingredients to represent the mechanical and neural tuning from the base to the apex of the cochlea.

Author contributions: A.S. and K.G. designed research, performed research, analyzed data, and wrote the paper.

The authors declare no conflict of interest.

This article is a PNAS Direct Submission. D.P.C. is a guest editor invited by the Editorial Board.

This open access article is distributed under [Creative Commons Attribution-NonCommercial-NoDerivatives License 4.0 \(CC BY-NC-ND\)](https://creativecommons.org/licenses/by-nc-nd/4.0/).

<sup>1</sup>To whom correspondence may be addressed. Email: grosh@umich.edu.

This article contains supporting information online at [www.pnas.org/lookup/suppl/doi:10.1073/pnas.1900695116/-DCSupplemental](https://www.pnas.org/lookup/suppl/doi:10.1073/pnas.1900695116/-DCSupplemental).

Published online June 20, 2019.

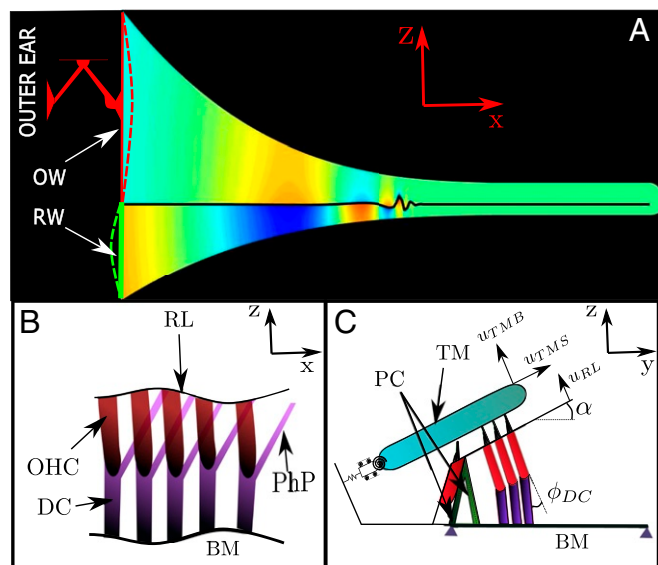


**Fig. 1.** (A) Schematic of the finite-element model of the guinea pig cochlea showing the variation of the height of the scala vestibuli and the scala tympani included in the finite-element model from base to apex based on areal measurements of the guinea pig cochlea (refs. 8 and 9 and *SI Appendix*). The fluid in the scalae is modeled as compressible and viscous and is coupled to the oval window (OW) and the round window (RW), which are modeled as flexible membranes with a single vibrational mode as shown with dashed lines. The response pattern due to acoustic stimulation at the stapes has been exemplified where the color shows the pressure distribution in the scalae and the displacement of the cochlear partition is shown with the black line separating the scalae. (B) The longitudinal ( $x$  direction) connectivity of the phalangeal processes (PhP) and the Dieter cell (DC) to the reticular lamina (RL) at an apical location (10) is included in the model. (C) The cross-section of the organ of Corti (OoC) in the model is shown. The RL pivots about the pillar cells (PC) through a torsional spring and makes an angle,  $\alpha$ , with the basilar membrane (BM). The axes of the outer hair cells (OHCs) are assumed to be perpendicular to the RL and make an angle of  $\phi_{DC}$  to the DCs which are taken to be perpendicular to the BM. The tectorial membrane (TM) is modeled as a longitudinally shear-coupled beam (11) connected to the limbal attachment through a torsion spring while the BM is modeled as an orthotropic plate. The fluid is coupled to the cochlear partition (described in refs. 12 and 13 and *SI Appendix*). The directions of the TM shear ( $u_{TMS}$ ), TM bending ( $u_{TMB}$ ), and the RL ( $u_{RL}$ ) motions are shown. The geometrical and stiffness parameters are based on morphological data wherever possible and are summarized in *SI Appendix* along with the electromechanical model of the cochlea.

## Results

**A Base-to-Apex Model of the Cochlea.** First, we compare the magnitude and phase of the BM gain (the frequency-dependent ratio of BM motion to stapes motion) computed from our model (Fig. 1 and *Materials and Methods*) to experimental BM gain at a basal location of the guinea pig cochlea. The calculated gain magnitude is shown in Fig. 2A and the phase is shown in Fig. 2B. The response location is 3.9 mm from the stapes, for which the frequency of highest response (the characteristic frequency [CF]) is 16.3 kHz. The solid blue line shows the BM gain for the active model, and the blue dashed line shows the BM gain for the passive model. The experimental BM gain (27) in response to 20-dB SPL stimulus (corresponding to the active model) is plotted using blue diamonds, and the BM gain from a 100-dB SPL stimulus in a dead animal (corresponding to the passive model) is plotted using blue circles. Both model and experimental gains have been normalized to their corresponding maximum passive gains. The model and experimental results show a remarkable correspondence, with the peak active BM response exhibiting a 27- to 30-dB increase over the peak passive BM response and a phase accumulation of around 2 cycles in the active case and 1 cycle in the passive case.

The model calculation of the magnitude of the RL gain for the 3.9-mm location is shown in Fig. 2C and the computed phase is shown in Fig. 2D, where the RL gain is the ratio of the RL motion to the stapes motion. The solid red line shows the RL gain spectrum for the active model and the corresponding passive model prediction is shown with the red dashed line. The active and passive BM gains from Fig. 2A and B are replotted in Fig. 2C and D for reference. In the passive model, the RL gain is similar to that of the BM, and the RL moves in phase with the BM at all frequencies. However, in the active model, the RL gain is 13 dB more than the passive RL gain at 0.5 CF, in stark contrast with the BM gain spectrum (Fig. 2A) where the active and passive BM response spectra overlap for frequencies at or below 0.5 CF, consistent with experimental observations (28, 29). In addition, the RL moves out of phase with the BM at frequencies lower than the CF (Fig. 2D, *Insets*), in agreement with the phase difference between the RL and the BM seen in experiments at low SPL in guinea pigs (30), gerbils (28), and mice (29). Hence, the model successfully recreates the dramatic difference between the RL and the BM gains at frequencies less than the CF, as well as the phase difference between the RL and the BM seen in experiments at low and high stimulus levels. Comparison of our model results with data from an independent experiment is shown in *SI Appendix, Fig. S5*.

The comparison between model and experimental results for the RL gain at more apical locations, 75%, 80%, 92%, and

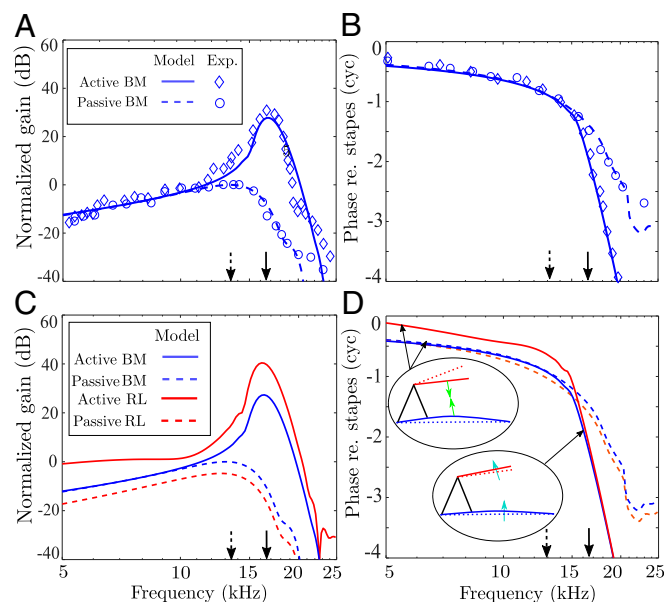


**Fig. 2.** Comparison of model predictions with experiments at 3.9 mm from the stapes in the guinea pig cochlea. (A and B) The gain and phase of the BM in the active (solid blue line) and passive (dashed blue line) model of the cochlea. The symbols show the response at 20 dB SPL and 100 dB SPL from ref. 27. (C and D) The prediction of the BM and the RL gain and phase for the active (solid lines) and the passive (dashed lines) model. The blue and red lines correspond to the BM and RL, respectively. In the active model, the RL moves out of phase with the BM at low frequencies and transitions to moving in phase close to the CF, whereas in the passive model the RL moves nearly in phase with the BM at all frequencies. In D, *Insets* illustrate the motion of the RL and BM in the active model at frequencies lower than the CF and at frequencies close to the CF. The active model predicts a RL gain that is 13 dB higher than that predicted by the passive model at 0.5 CF, in line with observations from refs. 29 and 31. The model and experimental gains have been normalized to their corresponding peak passive BM gains. The solid arrows show the CF of the location and the dashed arrows show the frequency of maximum gain for the passive BM. The only difference between the active and passive models is a reduction of mechano-electric transduction channel sensitivity to HB motion.





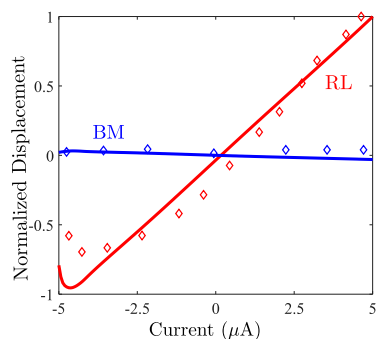


**Fig. 4.** Response of the RL and the BM to unipolar electrical stimulation in the scala media. The stimulus was chosen to be a  $-5\text{-}\mu\text{A}$  to  $5\text{-}\mu\text{A}$  current ramp, with onset and offset time of 5 ms. The solid blue line shows the model prediction of the BM displacement and the solid red line shows the model prediction of the RL displacement in response to the current sweep. The symbols show the data from Warren et al. (2). The displacements have been normalized to the peak RL displacement. The current-evoked RL motion is much higher than the BM motion due to the lower RL stiffness as well as the OoC geometry favoring RL over BM excitation by the OHCs. Further, the RL and BM displacements are antiphasic to each other because the force from the somatic electro-motility acts in opposite directions on the RL and the BM (32). The RL displacement at  $5\text{ }\mu\text{A}$  predicted by the model is  $150\text{ nm}$ ,  $3.75$  times larger than the  $40\text{-nm}$  RL displacement observed in the experiment.

the IHC HB (35–38). The computed ANF stimulus is inverted and normalized to its value at CF to estimate the normalized threshold frequency tuning curves (FTCs) shown in Fig. 5. The solid black lines in Fig. 5 *A–C* show the model prediction of the normalized threshold FTCs at 9 locations, 3 at each of the basal (Fig. 5*A*), middle (Fig. 5*B*), and apical (Fig. 5*C*) turns of the guinea pig cochlea. The red circles are normalized threshold FTCs from measured single ANF data obtained from the guinea pig cochlea (5). In the basal turn (Fig. 5*A*), the tip of the threshold ANF FTC is asymmetric, with the high-frequency limb much steeper than the low-frequency limb. Fig. 5*B* shows the model predictions and the experimental data from the middle turn, where the low-frequency limb of the FTC displays a significant reduction of slope compared with the FTCs at the base (4). At the apex (Fig. 5*C*), the model threshold FTCs transition to a more symmetric “V” shape, in line with the experimental data. Hence, our model successfully predicts the shape as well as the systematic transition of the low and high side slopes of the measured threshold ANF FTCs from base to apex (4).

**Duct Taper Leads to Physiological Tuning at Apex.** To test the effect of duct taper and macroscopic viscosity on the mechanical response, we simulated the response of the RL at an apical location (95% from the stapes) in cochleae under varying conditions of taper (Fig. 6, *Insets*) and macroscopic fluid viscosity. This location was chosen because the duct taper and macroscopic viscosity were found to be important only at apical locations (*Discussion* and *SI Appendix*, sections 5 and 6). In the simulations without duct taper, the height of the nontapered duct has been selected such that the scalae volume is the same for all models. The solid line in Fig. 6 shows the RL gain spectra for a model with a tapered geometry (Fig. 1 and Fig. 6, *Insets*) and macroscopic fluid viscosity (the nominal model, denoted as T-V) as simulated in Fig. 3*D*. We used an expanded frequency range down to  $10\text{ Hz}$  to clarify the differences between the models. The dashed line shows the RL gain spectra for a tapered cochlea without macroscopic fluid viscosity (denoted as T-NV), and the dotted line shows the RL gain spectra for a cochlea with a constant cross-sectional area (i.e., no taper) and without macroscopic fluid viscosity (denoted as NT-NV). Note that fluid viscosity in the subreticular space is included in all 3 mod-

els. All curves display a low-frequency filtering below  $80\text{ Hz}$  due to the shunting of the fluid pressure across the helicotrema. Both the NT-NV and T-NV models exhibit underdamped system resonances associated with apical reflections and the global motion of the entire organ of Corti (23). These nonphysiological modes of vibration are damped out in the T-V model. Further, the reduced duct height in the T-V and T-NV models led to increased fluid mass loading on the cochlear partition, reducing the CF of the location (39). Although both the T-V and the T-NV models predict a downward shift of the CF compared with the NT-NV model due to increased mass loading, only the T-V model displays a reduced CF as well as realistic low-frequency tuning.

## Discussion

**The Effect of Macroscopic Fluid Viscosity on Cochlear Tuning.** Oscillating flow of viscous endolymph and perilymph in the scalae results in the formation of boundary layers (BLs) at the walls of the duct as well as in the subreticular space (STS). Previous studies (33, 34, 40) have analyzed the dissipation due to the BLs in the STS, while others (41) have studied the effect of viscosity on the bulk or macroscopic fluid flow in the scalae ducts. In the present study, we concentrated on macroscopic viscous dissipation in the scalae because the accurate modeling of this effect in our model is one of the key factors that led to the transition from basal to apical dynamics (STS damping is used in all simulations). The combined thickness of the BL on the BM and the bony wall is given by  $d_{BL} = 2\sqrt{\nu/(\pi f)}$  (23, 42), where  $\nu$  is the kinematic viscosity of the fluid. In the basal turn of the guinea pig cochlea,  $d_{BL}$  is much smaller than the duct height at CF. Consequently, macroscopic fluid viscosity plays a minor role in the mechanical tuning at the base. However, at the apex, the duct height tapers significantly (Fig. 1*A* and *SI Appendix*, Fig. S2), resulting in  $d_{BL}$  being comparable to the duct height for frequencies at and below CF. The increased effect of macroscopic viscosity leads to overdamped motion of the BM and the RL (Fig. 6, T-V), resulting in a low-quality factor gain and the reduction of reflections from

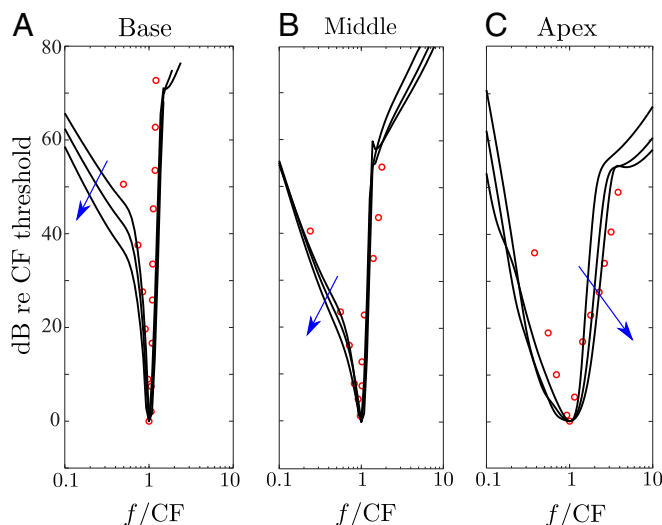


**Fig. 5.** Comparison of model prediction of threshold ANF FTC with experiments throughout the cochlea. The ANF FTCs predicted by the model are shown with solid black lines at the (A) basal (20%, 25%, and 30% the length of the cochlea), (B) middle (40%, 45%, and 50% the length of the cochlea), and (C) apical (85%, 90%, and 95% the length of the cochlea) turn of the guinea pig cochlea, normalized to the FTC threshold at the CF. At each turn, the blue arrows show the local base-to-apex transition at each location. All thresholds have been normalized to the threshold at the CF, and the frequency axis has been normalized to the CF at each location. The red circles show measurement of threshold ANF FTCs obtained from measurements in the guinea pig cochlea (5).

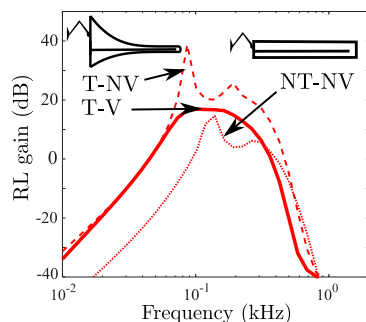


**Fig. 6.** Macroscopic viscosity and duct taper lead to physiological tuning at the apex. The RL gain spectrum at 95% for the model with taper and macroscopic viscosity (T-V model, schematic shown in *Left Inset*) is shown with the solid red line. The gain spectrum of the model with taper but without macroscopic viscosity (T-NV) is shown with dashed lines, and the gain spectrum for the model lacking both taper and macroscopic viscosity (NT-NV, schematic shown in *Right Inset*) is shown with dotted lines. Both the T-NV and NT-NV models display nonphysiological peaks due to apical reflections and system resonance. Further, the NT-NV model predicts a higher CF and band-pass characteristic. Only the T-V model correctly predicts the smooth band-pass spectrum seen in experiments. All 3 spectra show low-pass filtering below 80 Hz due to the shunting of the fluid pressure across the cochlear partition through the helicotrema.

the apex. Moreover, using the more physiologically realistic duct height in the model induces a greater fluid-loaded mass (as analytically shown in ref. 39) and lowers the CF compared with a cochlear model with constant cross-sectional area, a result we also confirmed using finite-element simulations (compare Fig. 6, T-NV and NT-NV). The combined effect of macroscopic fluid viscosity and fluid mass loading on the cochlear partition leads to the smooth and broad gain spectrum observed *in vivo* at the apex and creates a natural transition between the tuning at the basal and that at the apical turns of the cochlea (Fig. 5 and *SI Appendix*, Fig. S6). While the exact purpose of such a transition in the mammalian cochlea remains unclear, we speculate that the enhanced viscous effects at the apex could have created an evolutionary advantage by supporting higher cochlear gains without compromising stability, resulting in a broader dynamic range of hearing. A systematic study of the effect of macroscopic viscosity and duct height at different locations along the cochlear spiral is included in *SI Appendix*.

**The Organ of Corti Cytoarchitecture Significantly Impacts the BM Gain.** In addition to macroscopic fluid viscosity, the cytoarchitecture of the organ of Corti (OoC) influences the effectiveness of somatic electromechanical forces in modulating the vibrations of the BM and the RL. While orientation of the cytoarchitecture in the longitudinal direction (i.e., base-to-apex direction; Fig. 1*B*) is included in our model and has been studied extensively by others (43), our study primarily focuses on the cellular orientation in the radial plane (Fig. 1*C*) and its role in cochlear mechanics. In this plane, the RL is pivoted at an angle (denoted as  $\alpha$  in Fig. 1*C*) with respect to the BM that varies from  $\sim 5^\circ$  at the base to  $36^\circ$  at the apex in the guinea pig cochlea (*SI Appendix*, Fig. S4). Similarly, the angle between the axes of the OHCs and the Dieter cells (DCs) ( $\phi_{DC}$  in Fig. 1*C*) varies along the length of the cochlea. The somatic electromechanical force generated by the OHC is transferred to the transverse motion of the BM through the DC and is proportional to the product of the cosines of the angle between the OHC-DC ( $\phi_{DC}$ ) and the DC-BM ( $\alpha - \phi_{DC}$ ). Because of this change in orientation, the effective somatic force on the BM decreases by about 20% from base to apex, a factor that can result in a reduction of BM gain up to 20 dB (12). However, the OHCs are approximately perpendicular to the RL throughout the cochlea, a favorable orientation for actuation via somatic motility. The effect of the modulation of the active process by the geometry can be quantified by the ratio

of the maximum gain of the active and the passive model for the RL and the BM, denoted by  $\delta_{RL}$  and  $\delta_{BM}$ , respectively. From our model calculations,  $\delta_{RL}$  varies from 45 dB at the base to 20 dB at the apex (Fig. 3), implying high nonlinear gain of the RL throughout the cochlear spiral. Similarly, calculation of  $\delta_{BM}$  at the base (Fig. 2*A*) yields a value of 30 dB, in line with the nonlinear gain seen in experiments at the base of the guinea pig cochlea (27). However,  $\delta_{BM}$  was calculated to be around 2 dB at the apex, indicating a near level independence of the somatic amplification at the apex. This result is consistent with the measured BM gain at the apex which is nearly linear in response to sounds from 40 dB to 100 dB SPL (2). Further, the experimental and theoretical responses to electrical stimulation also demonstrate that somatic motility preferentially moves the RL over the BM at the apex (Fig. 4). Finally, the correlation of nonlinear gain and cochlear geometry is further exemplified by the mouse cochlea where the axes of OHCs are oriented nearly perpendicular to the BM over the entire length of the cochlea (44). Experimental observations show that, unlike in guinea pigs, the compressive nonlinearity in the BM gain spectrum in mice is greater than 20 dB throughout the cochlea (26, 45). This lends credence to our conclusion that the transition of the geometry of the organ of Corti plays a major role in reducing the effect of nonlinear compression of the BM motion at the apex of the guinea pig cochlea.

#### Different Factors Shape Threshold Neural Response at Base and Apex.

Comparison of Figs. 2*A* and 5*A* shows that the shape of the mechanical tuning (roughly the inverse of the gain function at low levels) is similar to that of the threshold neural tuning at the base of the guinea pig cochlea. This is because the high-pass filtering associated with the fluid coupling between the radial shear of the TM and the IHC HB (33, 34, 40), as well as the high-pass filter associated with the MET channel adaptation (35–37), has corner frequencies much lower than the CF in the basal turn. Consequently the basal threshold FTCs are primarily shaped by the mechanical dynamics of the organ of Corti (1, 46). However, in the apical turn, the model predicts that each of the high-pass filters associated with the STS fluid–HB coupling and the MET channel adaptation filter contributes a slope of 6 dB per octave for the low-frequency limb of the threshold ANF FTC (Fig. 5*C*) as discussed in refs. 21 and 47. An additional 6 dB per octave roll-off in the ANF filter is present for frequencies below the cut-in of the high-pass filter associated with the shunting of the acoustic pressure at the helicotrema (at around 80 Hz in our model, as seen in Fig. 6). The helicotrema cut-in frequency shifts to a higher frequency when the cochlear walls are fenestrated at the apex for measurement (as in refs. 3 and 48) or in species with larger helicotrema (21).

**Improvements and Suggested Future Modeling Work.** We have presented results from a physiologically based model of the cochlea that replicates the mechanical responses to acoustic and electrical stimuli over the entire length of the spiral and predicts ANF thresholds. Like most models that use a simplified geometry, the helicotrema was modeled as an opening in the cochlear partition at the apical end. However, the *in vivo* geometry of the helicotrema is complex and warrants more detailed 3D finite-element modeling, especially to model the response below 100 Hz. In addition, instead of incorporating the cochlear compression through a fully nonlinear formulation, we have used the quasi-linear approach to connect our active and passive linearized models of the cochlea to the response of the *in vivo* cochlea to low and high SPLs, respectively, as in other models such as refs. 13 and 17. This is related to the EQ-NL theorem (49) and has been shown to be true for pure tone stimuli (50). Finally, only the Couette flow was included in the STS, and other modes of fluid structure interaction (51) were not modeled due to the additional complexity. However, these modes might play an important role in predicting the nontip response in the threshold ANF FTCs (52).

## Materials and Methods

We have used a 2.5D hybrid finite-element model of the guinea pig cochlea (e.g., ref. 13) that incorporates physiological parameters based on measurements in the guinea pig or similar mammals. The scalae have been modeled as tapered prismatic ducts, as shown in Fig. 1, to accommodate the change in area observed in anatomical measurements of the guinea pig cochlea (9). The BM has been modeled as an orthotropic plate (13, 53), and the TM has been modeled as a longitudinally coupled viscoelastic beam (13). The kinematics and dynamics are derived from a Lagrangian formulation as

- M. A. Ruggero, S. S. Narayan, A. N. Temchin, A. Recio, Mechanical bases of frequency tuning and neural excitation at the base of the cochlea: Comparison of basilar-membrane vibrations and auditory-nerve-fiber responses in chinchilla. *Proc. Natl. Acad. Sci. U.S.A.* **97**, 225–243 (2000).
- R. L. Warren *et al.*, Minimal basilar membrane motion in low-frequency hearing. *Proc. Natl. Acad. Sci. U.S.A.* **113**, E4304–E4310 (2016).
- A. Recio-Spinoso, J. S. Oghalai, Mechanical tuning and amplification within the apex of the Guinea pig cochlea. *J. Physiol.* **595**, 4549–4561 (2017).
- A. N. Temchin, N. C. Rich, M. A. Ruggero, Threshold tuning curves of chinchilla auditory-nerve fibers. I. Dependence on characteristic frequency and relation to the magnitudes of cochlear vibrations. *J. Neurophysiol.* **100**, 2889–2898 (2008).
- E. F. Evans, The frequency response and other properties of single fibres in the Guinea-pig cochlear nerve. *J. Physiol.* **226**, 263–287 (1972).
- N. P. Cooper, W. S. Rhode, Nonlinear mechanics at the apex of the Guinea-pig cochlea. *Hear. Res.* **82**, 225–243 (1995).
- C. A. Shera, J. J. Guinan, A. J. Oxenham, Otoacoustic estimation of cochlear tuning: Validation in the chinchilla. *J. Assoc. Res. Otolaryngol.* **11**, 343–365 (2010).
- I. U. Teudt, C. P. Richter, The hemicochlea preparation of the Guinea pig and other mammalian cochleae. *J. Neurosci.* **162**, 187–197 (2007).
- C. Fernández, Dimensions of the cochlea (Guinea pig). *J. Acoust. Soc. Am.* **24**, 519–523 (1952).
- D. E. Zetes, J. A. Tolomeo, M. C. Holley, Structure and mechanics of supporting cells in the Guinea pig organ of Corti. *PLoS One* **7**, e49338 (2012).
- N. Gavara, R. S. Chadwick, Noncontact microrheology at acoustic frequencies using frequency-modulated atomic force microscopy. *Nat. Met.* **7**, 650–654 (2010).
- S. Ramamoorthy, N. V. Deo, K. Grosh, A mechano-electro-acoustical model for the cochlea: Response to acoustic stimuli. *J. Acoust. Soc. Am.* **5**, 2758–2773 (2007).
- J. Meaud, K. Grosh, The effect of tectorial membrane and basilar membrane longitudinal coupling in cochlear mechanics. *J. Acoust. Soc. Am.* **127**, 1411–1421 (2010).
- S. T. Neely, A model of cochlear mechanics with outer hair cell motility. *J. Acoust. Soc. Am.* **94**, 137–146 (1993).
- J. Meaud, K. Grosh, Effect of the attachment of the tectorial membrane on cochlear micromechanics and two-tone suppression. *Biophys. J.* **106**, 1398–1405 (2014).
- K.-M. Lim, C. R. Steele, A three-dimensional nonlinear active cochlear model analyzed by the WKB-numeric method. *Hear. Res.* **170**, 190–205 (2002).
- H. Motallebzadeh, J. A. M. Soons, S. Puria, Cochlear amplification and tuning depend on the cellular arrangement within the organ of Corti. *Proc. Natl. Acad. Sci. U.S.A.* **115**, 5762–5767 (2018).
- R. Ghaffari, A. J. Aranyosi, D. M. Freeman, Longitudinally propagating traveling waves of the mammalian tectorial membrane. *Proc. Natl. Acad. Sci. U.S.A.* **104**, 16510–16515 (2007).
- I. Russell *et al.*, Sharpened cochlear tuning in a mouse with a genetically modified tectorial membrane. *Nat. Neurosci.* **10**, 215–223 (2007).
- M. Fleischer, R. Schmidt, A. W. Gummer, Compliance profiles derived from a three-dimensional finite-element model of the basilar membrane. *J. Acoust. Soc. Am.* **127**, 2973–2991 (2010).
- P. Dallos, Low-frequency auditory characteristics: Species dependence. *J. Acoust. Soc. Am.* **48**, 489–499 (1970).
- D. Mountain, A. Hubbard, D. Ketten, J. O'Malley, "The helicotrema: Measurements and models" in *Biophysics of the Cochlea: From Molecules to Models*, A. W. Gummer, E. Dalhoff, M. Nowotny, M. Scherer, Eds. (World Scientific, 2003), pp. 393–399.
- S. Puria, J. B. Allen, A parametric study of cochlear input impedance. *J. Acoust. Soc. Am.* **89**, 287–309 (1991).
- D. Manoussaki *et al.*, The influence of cochlear shape on low-frequency hearing. *Proc. Natl. Acad. Sci. U.S.A.* **105**, 6162–6166 (2008).
- T. Reichenbach, A. J. Hudspeth, A ratchet mechanism for amplification in low-frequency mammalian hearing. *Proc. Natl. Acad. Sci. U.S.A.* **107**, 4973–4978 (2010).
- H. Y. Lee *et al.*, Two-dimensional cochlear micromechanics measured in vivo demonstrate radial tuning within the mouse organ of Corti. *J. Neurosci.* **36**, 8160–8173 (2016).
- E. de Boer, A. L. Nuttall, The mechanical waveform of the basilar membrane. III. Intensity effects. *J. Acoust. Soc. Am.* **107**, 1497–1507 (2000).
- W. He, D. Kemp, T. Ren, Timing of the reticular lamina and basilar membrane vibration in living gerbil cochleae. *eLife* **7**, e37625 (2018).
- T. Ren, W. He, D. Kemp, Reticular lamina and basilar membrane vibrations in living mouse cochleae. *Proc. Natl. Acad. Sci. U.S.A.* **113**, 9910–9915 (2016).
- F. Chen *et al.*, A differentially amplified motion in the ear for near-threshold sound detection. *Nat. Neurosci.* **14**, 770–774 (2011).
- D. Zha *et al.*, In vivo outer hair cell length changes expose the active process in the cochlea. *PLoS One* **7**, e32757 (2012).
- F. Mammano, J. F. Ashmore, Reverse transduction measured in the isolated cochlea by laser Michelson interferometry. *Nature* **365**, 838–841 (1993).
- A. Sasmal, K. Grosh, The competition between the noise and shear motion sensitivity of cochlear inner hair cell stereocilia. *Biophys. J.* **114**, 1–20 (2018).
- D. M. Freeman, T. F. Weiss, Superposition of hydrodynamic forces on a hair bundle. *Hear. Res.* **48**, 1–15 (1990).
- A. J. Ricci, H. J. Kennedy, A. C. Crawford, R. Fettiplace, The transduction channel filter in auditory hair cells. *J. Neurosci.* **25**, 7831–7839 (2005).
- A. W. Peng, T. Effertz, A. J. Ricci, Adaptation of mammalian auditory hair cell mechanotransduction is independent of calcium entry. *Neuron* **80**, 960–972 (2013).
- E. A. Stauffer, J. R. Holt, Sensory transduction and adaptation in inner and outer hair cells of the mouse auditory system. *J. Neurophysiol.* **98**, 3360–3369 (2009).
- S. Jia, P. Dallos, D. Z. Z. He, Mechano-electric transduction of adult inner hair cells. *J. Neurosci.* **27**, 1006–1014 (2007).
- C. R. Steele, L. A. Taber, Comparison of WKB calculations and experimental results for three-dimensional cochlear models. *J. Acoust. Soc. Am.* **65**, 1007–1018 (1979).
- S. Prodanovic, S. Gracewski, J.-H. Nam, Power dissipation in the subtectorial space of the mammalian cochlea is modulated by inner hair cell stereocilia. *Biophys. J.* **108**, 479–488 (2015).
- Y. Wang, C. R. Steele, S. Puria, Cochlear outer-hair-cell power generation and viscous fluid loss. *Sci. Rep.* **6**, 19475 (2016).
- P. K. Kundu, I. M. Cohen, D. R. Dowling, *Fluid Mechanics* (Academic Press, 2016).
- Y. J. Yoon, C. R. Steele, S. Puria, Feed-forward and feed-backward amplification model from cochlear cytoarchitecture: An interspecies comparison. *Biophys. J.* **100**, 1–10 (2011).
- J. A. M. Soons, A. J. Ricci, C. R. Steele, S. Puria, Cytoarchitecture of the mouse organ of Corti from base to apex, determined using in situ two-photon imaging. *J. Assoc. Res. Otolaryngol.* **16**, 47–66 (2015).
- S. S. Gao *et al.*, Vibration of the organ of Corti within the cochlear apex in mice. *J. Neurophysiol.* **112**, 1192–1204 (2014).
- S. S. Narayan, A. N. Temchin, A. Recio, M. A. Ruggero, Frequency tuning of basilar membrane and auditory nerve fibers in the same cochleae. *Science* **282**, 1882–1884 (1998).
- M. A. Ruggero, A. N. Temchin, The roles of the external, middle, and inner ears in determining the bandwidth of hearing. *Proc. Natl. Acad. Sci. U.S.A.* **99**, 13206–13210 (2002).
- W. Dong, N. Cooper, An experimental study into the acousto-mechanical effects of invading the cochlea. *J. R. Soc. Interf.* **6**, 561–571 (2006).
- E. de Boer, Connecting frequency selectivity and nonlinearity for models of the cochlea. *Aud. Neurosci.* **3**, 377–388 (1996).
- J. Meaud, K. Grosh, Response to a pure tone in a nonlinear mechanical-electrical-acoustical model of the cochlea. *Biophys. J.* **102**, 1237–1246 (2012).
- M. Nowotny, A. W. Gummer, Nanomechanics of the subtectorial space caused by electromechanics of cochlear outer hair cells. *Proc. Natl. Acad. Sci. U.S.A.* **103**, 2120–2125 (2006).
- H. Nam, J. J. Guinan, Non-tip auditory-nerve responses that are suppressed by low-frequency bias tones originate from reticular lamina motion. *Hear. Res.* **358**, 1–9 (2018).
- S. Liu, R. D. White, Orthotropic material properties of the gerbil basilar membrane. *J. Acoust. Soc. Am.* **123**, 2160–2171 (2008).
- L. Cheng, Y. Li, K. Grosh, Including fluid shear viscosity in a structural acoustic finite element model using a scalar fluid representation. *J. Comp. Phys.* **247**, 248–261 (2013).